Available online at www.sciencedirect.com

SciVerse ScienceDirect

Procedia Environmental Sciences 18 (2013) 384 – 390

Procedia Environmental Sciences

2013 International Symposium on Environmental Science and Technology (2013 ISEST)

Structural and surface effect of MnO_2 for low temperature selective catalytic reduction of NO with NH_3

Yue Peng, Huazhen Chang, Yun Dai, Junhua Li*

State Key Joint Laboratory of Environment Simulation and Pollution Control, School of Environment, Tsinghua University, Beijing 100084, China

Abstract

α- and β-MnO_2 with different phase structures were prepared by hydrothermal method and investigated for low temperature SCR. The α-MnO_2 catalyst showed higher activity than the β-MnO_2 catalyst at low temperature region. Characterization results revealed that the activity predominately depended on the tunnel (or layer) structure and surface chemisorbed oxygen rather than BET surface area, crystallinity, surface Mn^{4+}/Mn^{3+} ratio and redox property. α-MnO_2 showed the highest activity on account of [2×2] tunnel and the most surface oxygen to promote the NH_3 adsorption and activation. β-MnO_2 exhibited less activity because of [1×1] tunnel structure and little surface absorbed oxygen. Further, DFT calculations were used to model the clean and defect surface as well as the NH_3 adsorptions on the tunnels of α- and β-MnO_2 model surfaces.

Keywords: MnO_2; phase structure; tunnel; DFT; SCR; low temperature

1. Introduction

Nitrogen oxides (NO_x) emitted from stationary and mobile sources are major air pollutants, contributing to acid rain, photochemical smog, ozone depletion and fine particle pollution [1]. One of the most promising technologies for removal these pollutants from diesel engines is the selective catalytic reduction (SCR) of NO with NH_3. The commercial catalysts of industrial for the stationary sources are mainly V_2O_5-WO_3/TiO_2, however, the toxicity of vanadium species, high activity for the oxidation of SO_2 to SO_3 and narrow temperature window restrained their extensive applications; Fe-ZSM5 have been studied widely for the diesel vehicles engines, however, low activities at low temperature and poor hydrothermal durability at high temperature were still remained [2, 3]. Thus, the development of environmental benign catalysts with vanadium-free and high activity at low temperature is imperative to

* Corresponding author. Tel.: 86-010-62771093; fax: +86-010-62771093.
E-mail address: lijunhua@tsinghua.edu.cn.

doi:10.1016/j.proenv.2013.04.051

human beings and researchers.

Recently, great progress and development have been made in nanocrystal (NC) heterogeneous catalysis. The NC can be synthesized with various size and shape to enhance the activity of a specific catalytic reaction [4]. That is to say the catalytic properties of materials are sensitive to the shape of the NC (exposed well-defined facets). The utilizations of CeO_2, CuO and Co_3O_4 etc. continues to grow rapidly in the wide range of chemical reactions, and a direct relationship between the concentration of active sites and exposed crystal-plane for the CO or CH_4 oxidation [5–7]. On the other hand for the SCR reaction, there exists a debate about the reaction mechanism on vanadium-based catalysts at 300℃: Ramis proposed that an amide (NH_2) species resulting in catalyst reduction, while Topsøe suggested that NH_3 could be reactive only when adsorbed on the Brønsted acid site (NH_4^+) [2, 8]. Moreover, the mechanism for other catalysts such as metal oxides or zeolites were still not clear, the divergence was mainly focused on the rate-determine step at different temperature: the activation of NH_3 or the oxidation of NO to NO_2 [9, 10].

The α- and β-MnO_2 nanowires were first synthesized by selected control hydrothermal method [11], and were used to catalytic oxidation CO [12]. α- and β-MnO_2 have [2 × 2] and [1 × 1] tunnel size orientated to [110], respectively. Tang et al studied the NH_3-SCR activities of β-MnO_2 and α-Mn_2O_3 nanorods [13], Tian et al synthesized different shape MnO_2 catalysts (tubes, rods and particles) to study the SCR activity [14], and they both attributed the higher activity to and attributed the high activity to the crystallinity, high reducibility and more strong acid sites. However, they did not construct the systematically relationship between structure, temperature and activity. In our work, we extensively investigated the structural sensitivity and temperature determination of SCR activities on α- and β-MnO_2 nanowires by a combination of experimental and DFT calculations.

2. Materials and Methods

The α- and β-MnO_2 catalysts were synthesized by traditional hydrothermal methods. Activity measurements were carried out in a fixed-bed quartz reactor using 200 mg catalysts. The mixed feed gas contained 1000 ppm NO, 1000 ppm NH_3, 2 vol. % O_2 and N_2 as the balance gas, the total flow rate was 200 mL/min. The concentration of NO, NO_2 N_2O and NH_3 was measured by an FTIR gas analyzer. The crystal structure was determined by using an X-ray diffractometer (XRD) (Rigaku, D/max-2200/PC) between 10 ° and 80 ° at a step of 10 °/min, operating at 30 kV and 30 mA using CuKα radiation. XPS was obtained with an ESCALab220i-XL electron spectrometer from VG Scientific using 300 W AlKα radiations. TPR experiments were performed on a chemisorption analyser (Micromeritics, ChemiSorb 2720 TPx) under a 10% H_2 gas flow (50 mL/min) at a rate of 10 °C/min up to 1000 °C. Each sample was pre-treated at 300 °C in helium for 1 hour before testing. TPD experiments of NH_3 were carried out in a fixed-bed quartz reactor. 200 mg catalysts and 200 mL/min gas flow were used during the experiments.

All calculations are based on DFT, and were performed using the Material Studio modelling Dmol3 package [15]. Double-numerical plus polarization functions and GGA-PBE were used in all calculations [16, 17]. The spin polarization was applied and the real space cut-off radius was maintained as 4.2 Å. The core electrons were treated with all electrons relativistic. The α- and β-MnO_2 (001) models with 5 layers were obtained by cleaving the α- and β-MnO_2 unit cell, and all layers were fully relaxed. The vacuum regions were 10 Å thick. The Brillouin zone was sampled using a (2×2×1) Monkhorst Pack grid. The interactions between molecules and the surfaces are analyzed by the Mulliken charges. The surface oxygen vacancies forming energy (E_v) can represent the stability of surface oxygen. The E_v is calculated as follows:

$$E_v = E_{surface\text{-}v} + E_O - E_{surface} \quad (1)$$

where, $E_{surface\text{-}v}$ is the energy of surface with an O-vacancy, E_O is the energy of oxygen atom, and $E_{surface}$ is the total energy of clean surface. This formula assumes that the oxygen atoms leaving the surface combine to form the oxygen molecule. The adsorption energies (E_{ad}) of molecules are calculated for all possible active acid sites on the surfaces as follows:

$$E_{ad}=E_{surface}+E_{mole}-E_{mole/surface} \quad (2)$$

where, $E_{surface}$ is the energy of surface, E_{mole} is the energy of an isolated molecule that represents adsorbed molecules and $E_{mole/surface}$ is the total energy of the same molecule adsorbed on the surface. Note that a positive value for E_{ad} suggests stable adsorption [18].

3. Results and discussion

3.1. Crystallization and optimized models

Fig. 1(a) shows the XRD patterns of prepared α- and β-MnO_2 catalysts. They can be assigned to α-MnO_2 (JCPDS 44-0141) and β-MnO_2 (JCPDS 24-0735) [12]. Taking the intensities and half-widths of the diffraction peaks into account, β-MnO_2 had a higher crystallinity degree than α-MnO_2. In addition, the BET surface areas of α- and β-MnO_2 were 28.0, 14.0 m^2/g, respectively. Based on the results above, we construct the α- and β-MnO_2 models with (001) plane exposed (Fig. 1(b)). The optimized models indicate the different tunnel sizes (7.69 Å for α-MnO_2 model and 4.40 Å for β-MnO_2 model) are well agreement with experimental results [19, 20].

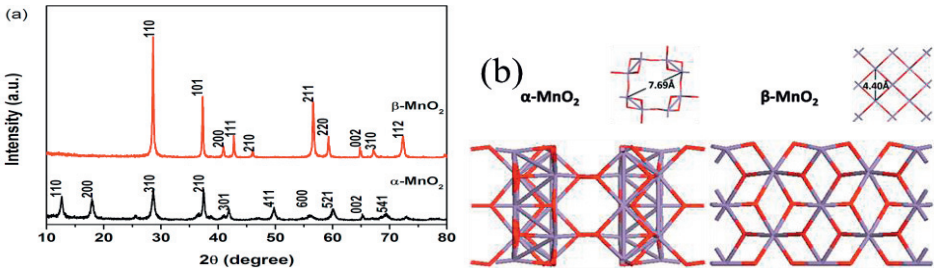

Fig. 1. (a) XRD patterns and (b) Top and front view of α- and β-MnO2 catalysts.

3.2. SCR activity

The NH_3-SCR activities of the α- and β-MnO_2 catalysts are shown in Fig. 2. During the temperature range from 60 to 200 °C, the α-MnO_2 catalyst exhibited higher NO conversions than the β-MnO_2 catalyst, and they can both yield 99% NO conversion at 200 °C then decreased with the temperature increasing. However, the activity of β-MnO_2 catalyst was higher than that of α-MnO_2 catalyst in the temperature range of 200-300 °C.

3.3. Redox property

Fig. 3(a) shows the H_2-TPR profiles. α-MnO_2 showed a shoulder peak around 275 ºC and a narrow peak located at 412 ºC, mainly attributing to the reduction of MnO_2 to Mn_3O_4, then to MnO [21], respectively. β-MnO_2 showed two peaks centered at 336 and 446 ºC, and the area ratio of the lower temperature peak to the higher one was about 2, indicating the reduction process of MnO_2 to Mn_3O_4, then to MnO [22]. The MnO_2 with longer Mn-O bonds has lower Mn-O strength, which can be reduced at

lower temperature. The surface Mn-O bond lengths of α- and β-MnO_2 (001) models were 1.94 and 1.88 Å, in agreement with the redox property [23]. Fig. 3(b) shows the O1s XPS spectra of α- and β-MnO_2 catalysts. The O1s peaks can be fitted into two peaks referred to the lattice oxygen at 529.3-530 eV (denoted as O_β) and the chemisorbed surface oxygen at 531.3-531.9 eV (denoted as O_α), respectively. As we know, the O_α is highly active in oxidation reaction due to its higher mobility than lattice oxygen O_β [24]. The corresponding concentrations of O_α were calculated from the relative areas of these sub-peaks and the results were 38.0% and 30.5% for α- and β-MnO_2 catalysts, indicating that α-MnO_2 obtained higher surface oxidative capability than β-MnO_2. O-vacancy can easily form on the MnO_2 surface, it is important to investigate the O-vacancy forming energy and gaseous molecules adsorption on these sites. First, we created an O-vacancy site by removing an oxygen atom from the surface, and then optimized the structure. The top views of the configurations are presented in Fig. 4. The E_v for the α-MnO_2 and β-MnO_2 models was determined to be 1.36 eV, 1.07 eV, respectively. It can be seen that the surface of α-MnO_2 (001) is more stable than β-MnO_2 (001).

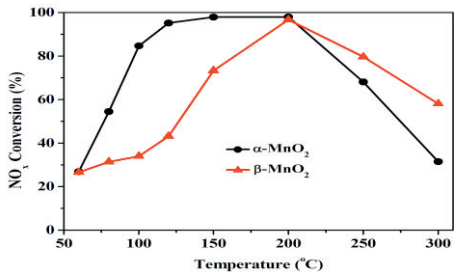

Fig. 2. SCR perormance of α- and β-MnO2 catalysts in the temperature range of 60 to 300 °C. Reaction conditions: NO 1000 ppm; NH3 1000 ppm; O2 2%; N2 balance; GHSV 38000 h-1.

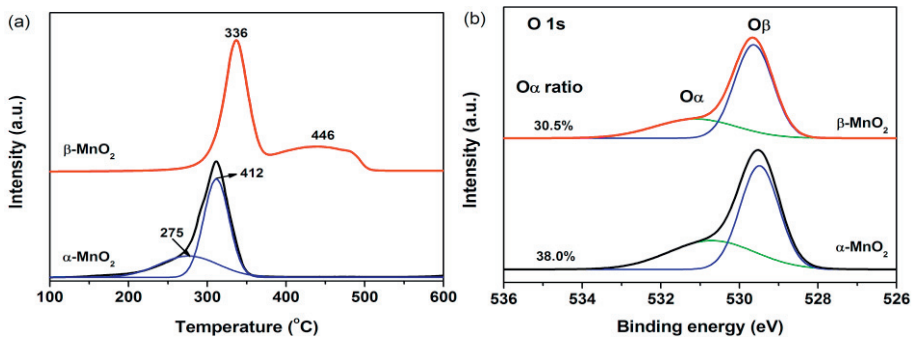

Fig. 3. (a) H2-TPR profiles and (b) XPS spectra of O 1s over α- and β-MnO2 catalysts.

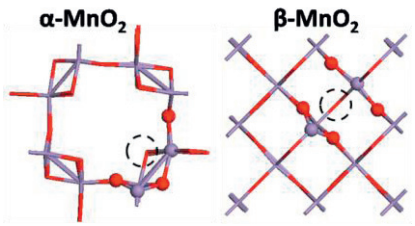

Fig. 4. Top view of optimized α- and β-MnO2 (001) models with O-vacancy sites indicated by black doted circle.

3.4. NH3 adsorption/desorption

To investigate the specific reaction, temperature programmed desorption (TPD) were utilized combined with DFT modelling. First we study the NH_3 adsorption/desorption on α- and β-MnO_2 catalysts (Fig. 5). The α-MnO_2 exhibited a wide, high peak located at 312 ºC, while for β-MnO_2, only a small peak at 282 ºC was detected. The results were indicating that α-MnO_2 could provide more NH_3 adsorption than β-MnO_2, however, the stability of NH_3 for α-MnO_2 is slightly greater than β-MnO_2. For DFT modeling, we simulated NH_3 adsorptions on both α- and β-MnO_2 (001) models, and listed the E_{ad} and charges of NH_3 on Table 1. The adsorption energy for α-MnO_2 is greater than that for β-MnO_2. The results indicated that NH_3 can bond with α-MnO_2 more stable. Mulliken charges of NH_3 indicated that more electrons of N could transfer from NH_3 molecule to the surface. Moreover, NH_3 molecule can adsorb not only on the (001) surface of α-MnO_2, but also in the [110] tunnel, while for β-MnO_2 based on the limitations of dynamic diameter, NH_3 molecule cannot adsorb in the tunnel. The adsorption configurations are shown in Fig. 6.

Table 1. Ead and charges of NH3 on α- and β-MnO2models.

Configuration[a]	Adsorption energy (eV)[b]	NH_3 charge[c]
A_L	2.03	+0.37
B_L	1.49	+0.28
A_B	0.81	+0.08
B_B	0.76	+0.06
A_V	1.94	+0.37
B_V	1.69	+0.21

[a] A denotes α-MnO_2 and B denotes β-MnO_2. The subscripts L, B, V are denotes as NH_3 adsorption on Lewis acid, Brönsted acid and O-vacancy site, respectively.
[b] calculated from formula (2)
[c] NH_3 charge are the sum of Mulliken charges calculated from every atoms of ammonia molecule.

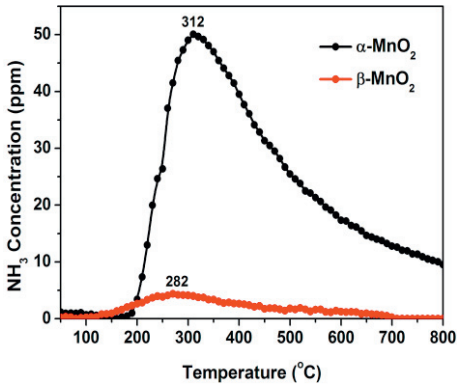

Fig. 5. NH3-TPD profiles of α- and β-MnO2 catalysts.

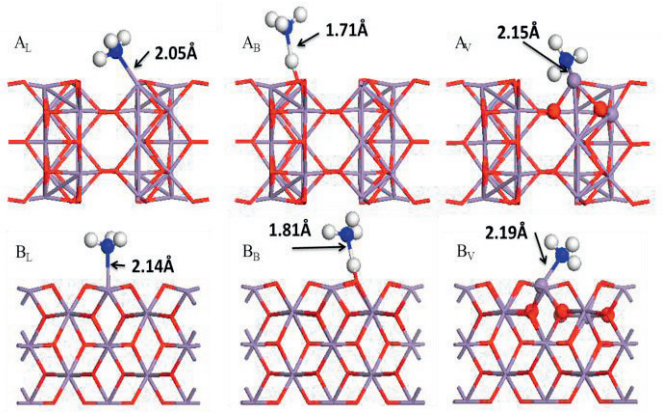

Fig. 6. The optimized configurations of NH3 adsorbed on α- and β-MnO2 models with the same sequences as Table 1.

4. Conclusions

α- and β-MnO_2 of different phase structures were prepared and investigated for the low temperature NH_3-SCR reaction. Results showed that the activity decreased in the order of α-MnO_2 > β-MnO_2 at low temperature. Characterization means of XRD, BET, XPS of O 1s and H_2-TPR indicated that the specific area, crystallinity, surface Mn^{4+}/Mn^{3+} ratio and redox capability were not the major factors to govern the catalytic activities of the two MnO_2 catalysts. The tunnel (or layer) structure and surface oxygen predominately controlled the catalytic activity. α-MnO_2 showed the best activity accounting for the [2×2] tunnel structure and surface chemisorbed oxygen to promote the adsorption and activation of NO and NH_3. β-MnO_2 exhibited poor activity because of the small [1×1] tunnel structure and little surface absorbed oxygen.

Acknowledgements

The authors gratefully acknowledge the financial support received from the national High−Tech Research and the Development (863) Program of China (2010AA065002, 2012AA062506) and the Science and Technology Department of Guangdong Province (2011A032303002).

References

[1] Liu Z, Woo S. Recent Advances in Catalytic DeNOx Science and Technology. *Catal. Rev.* 2006;**48**:43–89.
[2] Busca G, Lietti L, Ramis G, Berti F. Chemical and mechanistic aspects of the selective catalytic reduction of NOx by ammonia over oxide catalysts: A review. *Appl. Catal. B.* 1998;**18**:1–36.
[3] Brandenberger S, Kröcher O, Tissler A, Althoff R. The State of the Art in Selective Catalytic Reduction of NOx by Ammonia Using Metal–Exchanged Zeolite Catalysts. *Catal. Rev.* 2008;**50**:492–531.
[4] Zhou K, Li Y. Catalysis based on nanocrystals with well–defined facets. *Angew. Chem.* 2012;**51**:602–613.
[5] Liu X, Zhou K, Wang L, Wang B, Li Y. Oxygen Vacancy Clusters Promoting Reducibility and Activity of Ceria Nanorods. *JACS.* 2009;**131**:3140–3141.
[6] Leng M, Liu M, Zhang Y, Wang Z, Yu C, Yang X, Zhang H, Wang C. Polyhedral 50-Facet Cu_2O Microcrystals Partially Enclosed by {311} High–Index Planes: Synthesis and Enhanced Catalytic CO Oxidation Activity. *JACS.* 2010;**132**:17084–17087.
[7] Xie X, Li Y, Liu Z, Haruta M, Shen W. Low-temperature oxidation of CO catalysed by Co_3O_4 nanorods. *Nature* 2009;**458**:746–749.
[8] Topsoe Y, Topsoe H, Dumesic A. Vanadia/Titania Catalysts for Selective Catalytic Reduction (SCR) of Nitric-Oxide by Ammonia : I. Combined Temperature–Programmed in-situ FTIR and On–line Mass–Spectroscopy Studies. *J. Catal.* 1995;**151**:226–240.
[9] Qi G, Yang R. Performance and kinetics study for low-temperature SCR of NO with NH_3 over MnOx–CeO_2 catalyst. *J. Catal.* 2003;**217**: 434–441.
[10] Grossale A, Nova I, Tronconi E, Chatterjee D, Weibel M. The chemistry of the NO/NO_2–NH_3 "fast" SCR reaction over Fe-ZSM5 investigated by transient reaction analysis. *J. Catal.* 2008;**256**:312–322.
[11] Wang X, Li Y. Selected–Control Hydrothermal Synthesis of α– and β–MnO_2 Single Crystal Nanowires. *JACS.* 2002;**124**:2880–2881.
[12] Liang S, Teng F, Bulgan G, Zong R, Zhu Y. Effect of Phase Structure of MnO_2 Nanorod Catalyst on the Activity for CO Oxidation. *J. Phys. Chem. C* 2008;**112**:5307–5315.
[13] Tang X, Li J, Sun L, Hao J. Origination of N_2O from NO reduction by NH_3 over β–MnO_2 and α–Mn_2O_3. *Appl. Catal. B.* 2010;**99**:156–162.
[14] Tian W, Yang H, Fan X, Zhang X. Catalytic reduction of NOx with NH_3 over different–shaped MnO_2 at low temperature. *J. Hazard. Mater.* 2011;**188**:105–109.
[15] Delley B. From molecules to solids with the DMol3 approach. *J. Chem. Phys.* 2000;**113**:7756–7764.

[16] Becke A. Density–functional exchange–energy approximation with correct asymptotic behavior. *Phys. Rev. A* 1988;**38**:3098–3100.
[17] Perdew J, Burke K, Ernzerhof M. Generalized gradient approximation made simple. *Phys. Rev. Lett.* 1996;**77**:3865–3868.
[18] Bell S, Crighton J. Locating transition states. *J. Chem. Phys.* 1984;**80**:2464–2475.
[19] Yuan J, Li W, Gomez S, Suib S. Shape–controlled synthesis of manganese oxide octahedral molecular sieve three-dimensional nanostructures. *JACS.* 2005;**127**:14184–14185.
[20] Devarakonda M, Tonkyn R, Tran D, Lee J, Herling D. Modeling Species Inhibition of NO Oxidation in Urea-SCR Catalysts for Diesel Engine NOx Control. *J. Eng. Gas Turbines Power* 2011;**133**:092805.
[21] Wang C, Sun L, Cao Q, Hu B, Huang Z, Tang X. Surface structure sensitivity of manganese oxides for low-temperature selective catalytic reduction of NO with NH_3. *Appl. Catal. B.* 2011;**101**:598–605.
[22] Kapteijn F, Singoredjo L, Andreini A, Moulijn J. Activity and selectivity of pure manganese oxides in the selective catalytic reduction of nitric–oxide with ammonia. *Appl. Catal. B.* 1994;**3**:173–189.
[23] Devarakonda M, Tonkyn R, Tran D, Lee J, Herling D. Modeling Species Inhibition of NO Oxidation in Urea–SCR Catalysts for Diesel Engine NOx Control. *J. Eng. Gas Turbines Power* 2011;**133**:9
[24] Liu F, He H, Ding Y, Zhang C. Effect of manganese substitution on the structure and activity of iron titanate catalyst for the selective catalytic reduction of NO with NH_3. *Appl. Catal. B.* 2009;**93**:194–204.